Finite Observation Framework Predicts Tipping Points in Transient Dynamics

Sergio Cobo-López[1,2,3], Lucas J. Carbajal[4], Matthew Witt[1,5,6], Forest L. Rohwer[1,2], and Antoni Luque[1,4,7,*]

[1]Viral Information Institute, San Diego State University, San Diego, CA 92182, USA.
[2]Department of Biology, San Diego State University, San Diego, CA 92182, USA.
[3]Department d'Enginyeria Química, Universitat Rovira i Virgili, Tarragona, Catalonia, Spain.
[4]Department of Biology, University of Miami, Miami, FL 33146, USA.
[5]Department of Physics, San Diego State University, San Diego, CA 92182, USA.
[6]Holland Artificial Intelligence, San Diego, CA, USA.
[7]Department of Physics, University of Miami, Miami, FL 33146, USA.
[*]Corresponding author: antoni.luque@miami.edu

Abstract

The dynamics in any biogeochemical, ecological, and astronomical system are transient. Yet, predicting the occurrence of major dynamical shifts remains a challenge. To address this problem, we developed an efficient and pragmatic theoretical framework building on an overlooked fact: observers interacting with systems are bound to finite observational times and perceived changes. This finite observation principle defined a reference framework to diagnose the weight of different processes in the dynamics of a system and predict the critical values that will tip the dynamics to a new perceived regime. Tipping points were predicted to emerge due to the intrinsic finite nature of observations, leading to dynamic regimes increasing exponentially with the number of processes. However, for a given observer, only a subset of processes may be relevant in the dynamics, reducing the number of dynamic regimes perceived. The framework's predictions were tested by analyzing a classic predator-prey system with four processes parameterized in the context of bacteria (prey) and lytic bacteriophages (predator). Our approach predicted and recovered sixteen dynamic regimes, including the solutions for two non-trivial quasi-equilibrium dynamics. A Boolean model with only relevant processes generated dynamics within the observer's tolerance error, demonstrating the framework's accuracy. The approach introduced here simplifies the diagnosis of what processes in dynamical systems are relevant, when they become relevant,

and how these predictions depend on the observer. Thus, the observational framework provides a significant step forward in investigating and disentangling transient dynamics in any system.

Keywords

Transient dynamics, tipping points, critical transitions, Boolean dynamics, predator-prey systems.

INTRODUCTION

The emergence of marine photosynthetic bacteria triggered a transition from low to high oxygen in the atmosphere 2.5 billion years ago (Lyons et al., 2014; Margulis & Sagan, 1997). The disruption of the thermohaline circulation in the Atlantic during the Younger-Dryas period reversed the recovery from the last Glaciation period 12,000 years ago (Cheng et al., 2020; Scheffer, 2009). Even the periodic dance of planets around the Sun is predicted to derive into a chaotic dynamic in two billion years, likely leading to a collision between Earth, Mars, Venus, or Mercury (Hayes, 2007; Laskar & Gastineau, 2009), although by then the Sun will have expanded as a red star, likely engulfing these rocky planets (De et al., 2023). We live in a transient world. Yet, predicting when variables cross critical values that will tip the dynamics leading to a new dynamic regime is incredibly challenging (Scheffer, 2009; Seekell, 2016).

A common approach to studying transient dynamics is to assume that the system is stable near the equilibrium and that the emergence of another equilibrium state is driving the transition (Hastings et al., 2018; Panahi et al., 2023). However, no solid method exists for determining when such a transition may be triggered and how to predict the new emerging state (Scheffer, 2009; Scheffer et al., 2009). Theoretically, using two-timing approaches can help separate different timescale mechanisms, although, in practice, this method assumes asymptotic time for the slow process (Kevorkian & Cole, 1981; Strogatz, 2015). Alternatively, a dynamical system

can be integrated numerically, obtaining trajectories in the regions of interest (Bashkirtseva & Ryashko, 2018; Cairns et al., 2009; Cushing et al., 1998; Rabinovich et al., 2006; Rinaldi & Scheffer, 2000; Roach et al., 2017). However, not all the processes involved in the dynamic are relevant, adding a spectrum of sloppy parameters that are poorly constrained and tend to add spurious noise to the models, masking the underlying causes of regime shifts (Gutenkunst et al., 2007). Alternatively, empirical approaches have made significant progress in predicting tipping points using machine learning or statistical time series analysis (Oro et al., 2023), including the analysis of mean rates of state variables (Pedersen et al., 2020), the conditional heteroskedasticity to ecological systems (Pedersen et al., 2020; Seekell et al., 2011, 2012, 2013), or the identification of early-warning signals through resilience analysis (Bury et al., 2021; Ditlevsen & Ditlevsen, 2023; Scheffer et al., 2009). However, unlike the study of asymptotic dynamics or equilibria, a quantitative framework to classify and investigate transient dynamics mechanistically is still under development (Hastings et al., 2018; Strogatz, 2015).

Regime shifts in transient dynamics can range from gradual to dramatic and can be triggered by large to small changes in internal or external variables (Hastings et al., 2018; Scheffer, 2009). In general, during transient dynamics, the system variables can show a gradual or minor drift followed by a sudden and extensive change (Rocha et al., 2018). However, the study of dynamical systems is grounded on methods that rely on asymptotic equilibria and stability (Strogatz, 2015). To facilitate the characterization and prediction of regime shifts, we propose a new framework that assesses the weight of individual processes in the dynamics of a system. The approach builds on the empirical fact that any observer interacts and measures a system during a finite amount of time (observational time) and only perceives changes above a certain threshold (observational relevant change). Thus, an observer will perceive that a process

in a dynamic system is relevant if it changes substantially during the observation. Normalizing dynamic processes using the observational reference framework allowed us to identify processes above the observational rate that would be perceived as relevant. The critical values associated with processes becoming relevant or irrelevant led to tipping points that changed the perceived dynamics of the system. We illustrated the application of the observational framework using a classic predator-prey system in the context of bacteria (prey) and bacteriophage (predator). The analysis of this system confirmed the accuracy of the approach relying on relevant processes and recovered the number of predicted dynamic regimes and quasi-equilibrium solutions. The discussion section elaborates on how the basic premises of the observational framework can be immediately translated to more complex systems, providing a guide to diagnosing and predicting transient dynamics.

METHODS

Identification of dynamic regimes and tipping points in the observational reference framework. The observational framework was defined based on the relevant observational time Δt_{obs} and relevant observational change $\Delta A_{i,obs}$ for each agent (or observable dynamic variable) A_i (see Figure 1). Their ratio defined the relevant observable rate, $r_{i,obs} = \frac{\Delta A_{i,obs}}{\Delta t_{obs}}$. The dynamics of each agent A_i was defined as the net rate of change, summing the processes F_{ij}. Normalizing the rates using the relevant observable rate yielded the weight of each process $w_{ij} = \frac{F_{ij}}{r_{i,obs}}$. A process was interpreted as dynamically relevant if its weight was above one, $w > w_{th} = 1$, where w_{th} was the weight's threshold (tipping point). The values of the dynamic variables at the

tipping point were defined as the critical values, $A_{i,c}$,. Each dynamic regime was defined as a unique set of relevant processes. Figure 1 illustrates the key steps described above.

Dynamic regimes and tipping points in a Lotka-Volterra system for phage and bacteria. The bacteria (prey), $A_1 = B$, and a lytic bacteriophage (predator), $A_2=P$, dynamics were approximated using a standard Lotka-Volterra model (Weitz, 2016). The net rate of change of the bacterial population was defined by two processes: the bacteria growth rate, $F_{11}=F_g$, and the phage infection or predation pressure, $F_{12}=F_p$ (see differential equations in Figure 2a). The net rate of change of the phage population was also defined by two processes: the phage production or burst when lysing an infected cell, $F_{21}=F_b$, and the phage decay rate, $F_{22}=F_d$ (Figure 2a). The observational time was defined as $\tau = \Delta t_{obs}$, while the relevant observational change of phage and bacteria was set, respectively, to $\Delta B_{obs} = \alpha \cdot B$ and $\Delta P_{obs} = \alpha \cdot P$. Here α was the fraction of the population contributing to an observable, relevant change. The weights of each process and critical concentrations associated with tipping points were obtained following the prescriptions described in the previous section and are shared in the Results. The dynamic regimes were associated with different combinations of processes being relevant for the observer.

*Attractors of the dynamic regimes***.** The theoretical attractors were derived as the asymptotic solution ($\tau \to \infty$) of the differential equations defined by the subset of relevant processes associated with each dynamic regime. If a fixed point existed (making the rates of the system equal to zero), then the linear stability of the fixed point was evaluated by the eigenvalues of the Jacobian, following standard practices (Strogatz, 2015). The analysis is available in Supplementary File 1 (Tables S1 to S4).

Model parametrization. The range of values for the agents, parameters, and typical observational times in the model were obtained from the literature for both laboratory experiments and environmental studies (Anthenelli et al., 2020; Brum et al., 2016; K. Cheng et al., 2007; De Paepe & Taddei, 2006; Kannoly et al., 2023; Luque & Silveira, 2020; Silveira et al., 2021; Suttle & Chen, 1992). The values are summarized in Table 1. The specific contribution of each reference to the pool of values is provided in Supplementary File 2. In the numerical analysis, the observer's tolerance was set to $\alpha = 0.1$, that is 10% change with respect each population.

Numerical simulations. Case studies illustrating all predicted dynamic regimes in the observational framework were explored following the theoretical analysis shared in the Results section. This led to four sets of parameter values (one for each scenario), which were selected with a rationale capturing laboratory and environmental studies (Table 1). For scenarios predicted to produce quasi-equilibrium solutions, two sets of initial conditions were used, capturing quasi-equilibrium as well as transient trajectories. The system of differential equations was coded in Python and integrated with the *solve_ivp* function in *scipy* library (Virtanen et al., 2020). This function relying on the LSODA solver from the FORTRAN library odepack (Hindmarsh, 1983), which automatically switches between non-stiff and stiff solvers depending on the behavior of the equations (Petzold, 1983). The code developed to generate the simulations is available on GitHub (https://github.com/luquelab/needle-finder). The simulated dynamics (including populations, weights, and relevant processes) are provided in Supplementary File 3.

Error analysis of the predicted regimes. To test the accuracy of the observational framework, the full phage-bacteria model (Figure 2a) was compared with a dynamically adaptive Boolean model that integrated only the relevant processes in a regime. The adaptive differential

equation model was obtained by multiplying each process of the original model by a Heaviside step function ($\theta_i(w_i - w_{th})$) = 1 for $w_i \geq w_{th}$ and 0 otherwise), where w_i was the weight of the process *i* and w_{th} = 1 was the threshold. This differential equation was integrated for the same initial conditions, parameters, and methods as the full model. The error for each population was obtained as the absolute difference between the value from the full and adaptive models at each time step. The relative error was defined as the absolute error divided by the value of the full model. The combined error was defined as the average of the relative errors of the populations at each time step. Summary statistics were obtained for each regime, scenario, and overall simulation dynamics.

Analyzing the impact of adding a new process. The phage-bacteria model defined by the Lotka-Volterra equations was modified by adding a carrying capacity process associated with the competition between bacteria for resources (see modified equation in the Results section). The weight of the carrying capacity process w_K was obtained using the observational framework. Conditions associated with the quasi-equilibrium solution of the standard model were used to assess the impact of the process on the system (Table 1). The observational framework was used to predict the critical observational time needed to observe the impact of the carrying capacity process ($w_K > w_{th} = 1$). The full and adaptive models were simulated and compared to assess the errors of the observational framework.

RESULTS

The finite observable framework leads to general measurable predictions for dynamical systems.

Tipping points depend on the observer. The normalization of process *j*, F_{ij}, in the dynamics of agent *i* to the reference observational rate $r_i^{obs} = \frac{\Delta A_i^{obs}}{\Delta t^{obs}}$ defined the weight of each process $w_{ij} = \frac{F_{ij}}{r_i^{obs}}$ in the observer's reference framework (Figure 1). Here, Δt^{obs} was the relevant observational time, ΔA_i^{obs} the relevant observational change for the agent *i* (observable dynamic variable). A process was predicted to be relevant in the observational framework if its rate was similar or larger than the observational rate $|F_{ij}| \geq r_i^{obs}$. In terms of the weights, the *condition for relevance* was translated as follows:

$$\text{A process, } F_{ij}\text{, is relevant if its weight, } w_{ij} = \frac{F_{ij}}{r_i^{obs}}\text{, satisfies } |w_{ij}| \geq w_{th} = 1. \qquad \text{Eq. (1)}$$

Here, w_{th} was the critical threshold. The critical values of the variables and parameters leading to the threshold value $|w_{ij}^*| = w_{th} = 1$ (tipping point) were predicted to determine when a process switches from relevant to irrelevant or vice versa (Figure 1). Thus, for two observers subject to different observational rates, $r_i^{obs(1)} \neq r_i^{obs(2)}$, they will perceive different weights for the same process, $w_{ij}^{obs(1)} \neq w_{ij}^{obs(2)}$. Thus, they will perceive tipping points at different critical values. Moreover, for asymptotic observational times, $\Delta t^{obs} \to \infty$, or infinitely precise observational resolutions, $\Delta A^{obs} \to 0$, the perceived weight of a finite process is expected to be infinite, $w_{ij} \to \infty$, that is, the associated process will always be relevant, and no tipping points will exist. Therefore, tipping points are an emerging property of the finite observational reference of the observer.

The observable dynamic regimes increase exponentially with the number of processes. At any given time, only relevant processes should significantly impact the dynamics perceived by the observer. The changes in the dynamic variables can subsequently cross critical values, making an irrelevant process relevant or vice versa, activating new attractors that will drive the dynamics (Figure 1). Since each process could be either relevant or irrelevant, the number of dynamic regimes, *D*, that an observer can perceive was predicted to grow exponentially with the number of processes, M, in the system:

In a system with $M = \sum_{i=1}^{N} n_i$ processes there are $D \leq 2^M$ observable dynamic regimes. Eq. (2)

Thus, systems with more processes can lead to exponentially more complex observable dynamics. Alternatively, if a system remains in the same dynamic regime during the observational time, the asymptotic attractors during the observation would remain the same, leading the observer to perceive dynamics as more predictable or *quasi-steady*. If the dynamics remain in the same regime and the variables oscillate around or converge towards a constant value, the observer may interpret the system as being in *quasi-equilibrium*. In the limit case, where the value of dynamic variables remains within the relevant observable change, the observer may perceive the system as *quasi-static* (Figure 1).

The case study for a Lotka-Volterra model in the context of phage and bacteria confirmed the general predictions.

The observational framework predicted sixteen dynamic regimes distributed in four scenarios. The normalization of the phage and bacteria (Lotka-Volterra) model (Figure 2a) using the observational framework yielded the equation rates in terms of the weights, *w*, for the four processes (*M*=4) in the system, that is, bacterial growth (w_g) and phage predation (w_p)for the

bacterial rate of change, and the phage production or burst (w_p) and phage decay (w_d) for the phage rate of change:

$$\frac{\tau}{\alpha B}\frac{dB}{dt} = \underbrace{\frac{\tau\, r}{\alpha}}_{growth,\, w_g} - \underbrace{\frac{\tau\, a\, P}{\alpha}}_{predation,\, w_p} \qquad \text{Eq. (3)}$$

$$\frac{\tau}{\alpha B}\frac{dB}{dt} = \underbrace{\frac{\tau\, c\, a\, B}{\alpha}}_{burst,\, w_b} - \underbrace{\frac{\tau\, m}{\alpha}}_{decay,\, w_d}$$

Here, r was the bacterial intrinsic growth rate constant, a the adsorption-infection rate constant, c the phage burst size, and m the phage decay rate constant. The parameter α was the observational tolerance used in the relevant observational change, $\Delta B^{obs} = \alpha B$ and $\Delta P^{obs} = \alpha P$. For these observational changes, the weights for the growth rate, w_g, and phage decay, w_d, were constant in the dynamics for the observational framework, Eq. (3). These processes were predicted to be observable ($w > w_{th}=1$) for observational times $\tau \geq \tau_g = \alpha/r$ and $\tau \geq \tau_d = \alpha/m$, respectively. The weights for the predation, w_p, and phage burst (or production), w_b, depended on dynamical variables, respectively, the phage population, P, and the bacterial population, B, Eq. (3). Thus, the threshold (or tipping point), $w_{th} = 1$, predicted the critical concentrations $P_c = \alpha/(\tau\, a)$, and $B_c = \alpha/(\tau\, c\, a)$ for the predation and phage burst to become relevant processes, respectively. Since the weights for the growth, w_g, and decay, w_d, were constant in this reference observational framework, it was possible to explore the predicted sixteen, 2^4, dynamic regimes, Eq. (2), in four scenarios: Scenario 1 (relevant growth and irrelevant decay), Scenario 2 (irrelevant growth and relevant decay), Scenario 3 (relevant growth and decay), and Scenario 4 (irrelevant growth and decay). The theoretical asymptotic analysis of each regime (dynamic subsystem with a unique set of relevant processes) identified the attractors for each scenario as indicated in Tables S1 (Scenario 1), S2 (Scenario 2), S3 (Scenario 3), and S4 (Scenario 4) (see Supplementary File 1).

The attractors in each scenario consistently drove the dynamic trajectories obtained when exploring specific parameters related to different biological situations (Table 1) across the four scenarios (Figure 2b). As predicted in the attractor analysis, the system was observed to be in quasi-equilibrium when either all processes remained relevant, recovering the traditional periodic Lotka-Volterra solution (Figure 2b3), or all processes remained irrelevant, leading to a quasi-static solution (Figure 2b4).

Processes predicted to be relevant accurately reproduced the transient dynamics. The first biological scenario was investigated using parameters and observational times related to standard laboratory experiments for fast-growing bacteria, like *E. coli*, and lytic phages, like T4 phage (Table 1). The dynamics in these conditions showed an initial bacteria population increasing exponentially while the phage population remained relatively constant (Figure 3a); the phage then grew rapidly, and a sharp decline of the bacteria population followed; then the phage concentration stopped growing and remained constant until the end of the 14 hours of observation (Figure 3a). The analysis of the weights (Figure 3b) indicated that the bacterial growth process's weight, w_g, remained constant above the threshold value, $w_g = 126 > w_{th} = 1$; the decay remained constant but below the threshold, $w_d = 0.21 < 1$; the weights for the phage production (burst process) and phage predation on bacteria crossed the critical thresholds at three times (Figures 3b and 3c): at 1.06 h the phage burst became relevant ($B>B_c$ = $2.6\cdot10^3$ cells/ml), at 7.48 the predation process became relevant ($P>P_c$ = $1.3\cdot10^5$ phages/ml), and at 9.90 h the phage burst went back to irrelevant ($B<B_c$). The transient dynamics, thus, covered the four dynamic regimes (I, II, III, and IV) expected for Scenario 1 for relevant growth and irrelevant decay (Figure 2b1). The adaptive Boolean model, which only integrated relevant

processes ($w>w_{th}$), yielded dynamics that were visually indistinguishable from the full model (Figure 3a). The error varied across the regimes, yielding an average relative error (combined populations) of 2.26% (Figure 3d), with the bacterial population's most significant error in the fourth regime (mean error = 10.87%) and the phage in the third regime (mean error = 2.60%); see Figure 3d and Table S6.

To explore the opposite dynamic scenario (irrelevant bacterial growth and relevant phage decay), the parameters used were related to marine systems with slow-growing bacteria and fast phage decay occurring at the sea surface due to sunlight effects (see Table 1). The dynamics (Figure S1) illustrated the four initial regimes (V, VI, VII, and VIII) expected (Figures 2b2). The adaptive Boolean model integrating only relevant processes yielded a mean (combined) error of 0.42% with maximum errors of 0.76% for bacteria and 0.31% for phage (Figure S1d and Table S6).

Two quasi-equilibrium regimes are observable in the Lotka-Volterra dynamics. The quasi-equilibrium dynamic predicted when all processes were relevant (Table S3) was recovered in Scenario 3, using initial conditions that remained above the critical concentrations for both bacteria and phage (Figures 2b3 and 4a). The parameters for Scenario 3 were similar to the marine populations in Scenario 2 but assumed a faster-growing bacterial population, which is possible in enriched environments like habited coastal ecosystems (Table 1). The system oscillated around the classical theoretical equilibrium of the Lotka-Volterra system (Figure 4a). Since all the processes were relevant (Figure 4b), the adaptive Boolean model yielded no errors (Table S5). Alternatively, for initial conditions where at least one of the populations was below the critical concentrations, not all the processes were initially relevant, generating more abrupt

oscillations around the equilibrium (Figures 4c and 2b3). The crossing of critical concentrations led to alternating regimes, where all processes were relevant during a fraction of the observation (Figures 4d and 4e). The adaptive Boolean model integrating relevant processes accurately reproduced the dynamics of the full model (Figure 4c), yielding a mean combined error of 0.74%, where the errors in the bacterial and phage populations oscillated depending on the regime (Figure 4f).

The second quasi-equilibrium situation was predicted when all processes were irrelevant, and all populations were predicted to remain quasi-static with values similar to the initial conditions (Table S4). This prediction was captured as part of Scenario 4 (Figure 2b4). The parameters used resemble the environmental values of Scenario 2, using slow phage decay instead, a situation that is plausible in the deep ocean (Table 1). The observational time was shortened to be similar to Scenario 1; the slow-growing bacteria and slow-decaying phage were observed under laboratory times. For initial conditions below the critical concentrations ($B_0 < B_c = 5.1 \cdot 10^3$ cells/ml and $P_0 < P_c = 2.6 \cdot 10^5$ phages/ml), the system remained in a quasi-static state for the observational time with a mean combined error on the adaptive dynamics of 0.09% (Figures 2b4 and S2 and Table S5). Starting initial conditions above the critical bacterial concentration led to transient dynamics crossing different regimes with a mean combined error of the adaptive model of 2.06% (Figures 2b4 and S2 and Table S5).

The observational framework accurately predicts when newly added processes are relevant.

297 Adding a bacterial competition process $-\frac{rB^2}{K}$, where *K* was the carrying capacity, in the phage
298 and bacteria model (Figure 5a) introduced, theoretically, an asymptotic global stable
299 equilibrium $B_{eq} = \frac{m}{c \cdot a}\ and\ P_{eq}\ = \frac{r}{a} \cdot \left(1 - \frac{B_{eq}}{K}\right)$. However, the observational framework predicted
300 that the effect should be only observable if its weight, w_K (Figure 5a), was relevant ($w_K > w_{th} = 1$).
301 This was explored using the conditions for quasi-equilibrium from Scenario 3 and setting up the
302 carrying capacity to $K = 10^9 \frac{cells}{ml}$, a reasonable value in coastal conditions (Table 1). The
303 dynamics obtained (Figure 5b) were similar to the case without carrying capacity (Figure 4a)
304 because the carrying capacity's weight remained below the threshold. $w_K\ =\ \tau \cdot r \cdot \frac{B}{K \cdot \alpha} \sim 0.18\ <$
305 $w_{th}\ =\ 1$ (Figure 5a). The adaptive Boolean model produced a dynamic that was visually
306 indistinguishable from the full model but yielded a mean combined error of 0.98% (Figure 5a
307 and Table S5). Alternatively, the observational framework predicted that for the carrying
308 capacity to be relevant, the observational time would have to be $\tau' \geq\ \tau_0' = \frac{K * \alpha}{r * B}$. This prediction
309 was explored using an observational time $\tau' =\ 30{,}000\ h\ >\ \tau_0' = 10{,}000\ h$, which revealed the
310 expected effect of the carrying capacity: the amplitudes of the oscillations were dampened as the
311 dynamics converged toward the expected asymptotic global stable equilibrium (Figure 5c). In
312 this case, all processes remained relevant throughout the dynamics, and the adaptive Boolean
313 model yielded no errors (Figure 5b).
314
315 **DISCUSSION**
316
317 Our results indicate that given a dynamical model, only processes relevant to the observer's
318 framework matter in describing the dynamics. Processes become relevant or irrelevant

dynamically when their variables cross well-defined critical values, representing tipping points that move the system through different dynamic regimes. The numerical exploration of this prediction for the bacteria (prey) and bacteriophage (predator) system illustrates the accuracy of the observational reference framework. A vital consequence of this framework is that even a relatively small system composed of four dynamic processes comprises sixteen (2^4) dynamic regimes, each defined by the corresponding relevant processes. Exploring the whole space of dynamic regimes might not be feasible for larger models since it is predicted that its size exponentially scales with the number of dynamic processes considered as predicted by Eq. (2). However, for a finite observational time, the number of dynamic regimes (sets of relevant processes) covered is expected to remain strongly constrained base on the specific parameter values associated with the system during the observational time. Thus, despite the total number of possible dynamics may not be feasible to be studied, the subset of dynamic regimes observed that would benefit from analysis will usually represent a much smaller fraction and increase linearly with the observational time. In other words, our method provides a tool to characterize local regimes on any system despite its complexity.

The observational framework can generate some potential paradoxes that are worth noting. For example, in Scenario 1 studied here (Figure 3), the dynamic regime II was characterized by the phage production process being relevant, while the bacteria infection (or phage predation) was not. This apparently violates causality because bacterial infection is needed to produce phages. However, from the observer's point of view, the number of bacteria killed by the phage is not substantial (perceptible) because the phage concentration is below its critical value. In contrast, the phage production is significant because the bacteria concentration is above the critical value. Without knowledge of the mechanism underlying the dynamics, this

observation could lead to the wrong causal interpretation. Yet, the observational framework helps reconcile this puzzling regime of the dynamics. Implementing it upfront to study empirical systems could provide a more nuanced and cautionary interpretation of the potential mechanistic relationship underlying the dynamics, even when apparent causality is not obvious.

The accuracy within the observational framework achieved with the Boolean model demonstrates that the dynamics are dominated by local attractors associated with the subset of relevant processes at a given time (Figure 2). This indicates how dynamic regime changes do not require distant global attractors to steer the dynamics. At the same time, the relation between relevant processes and finite observational factors indicates how the perception of the dynamics and its regimes is intrinsically associated with the observer. Different observational times change the outcome of the dynamics and the processes that are necessary to approximate the full dynamics, as observed when investigating the effect of the carrying capacity (Figure 5). This is a subtle but key point when investigating natural systems because the existence of well-described mechanisms does not imply that they will be relevant. Thus, it is necessary to incorporate observational times and relevant changes to rigorously assess when mechanisms matter in a system.

In short, the observational framework is a pragmatic approach to forecasting tipping points and regime shifts in dynamical systems. The weights of processes act as early warning signals as they approach their tipping points in a similar way as the resilience does in other approaches (Bury et al., 2021; Ditlevsen & Ditlevsen, 2023; Folke et al., 2010; Scheffer, 2009). However, within the observational framework, critical transitions occur when dynamic terms become relevant or irrelevant. Each set of processes defines different attractors that characterize the dynamics in a regime. As an attractor steers the system, it may cross tipping points, making

other processes relevant or irrelevant, changing the attractor and steering the dynamics to a new direction. Thus, the observer may perceive systems to display rich dynamics and even apparent multistable dynamics despite the classical asymptotic approach, which may predict a single global equilibrium. Overall, the observational framework opens the door to an efficient protocol to forecast regime shifts in real systems: obtain data of the system for a time shorter than the observational timescale; assess the weights of the plausible processes; determine active processes and tipping points; predict dynamic shifts; be prepared for the shift or act to prevent it.

ACKNOWLEDGEMENTS

The authors thank the invaluable insights from Joan Roughgarden, the Biomath working group at San Diego State University, and Alexander V. Alekseyenko (Medical University of South Carolina) for the fruitful discussions at New York University that planted the seed of this project. The authors also acknowledge the crucial influence in the current study of the Master Thesis from Matt Witt carried under the supervision of Antoni Luque at San Diego State University (Witt 2019). The authors acknowledge the funding support of different agencies that made the research published here possible. The National Science Foundation awards #1951678 and #2424579 supported the research of A.L. and L.J.C. The Gordon and Betty Moore Foundation grant GBMF9871 (https://doi.org/10.37807/GBMF9871) supported the research of A.L. and F.R. The Gordon and Betty Moore Foundation grant GBMF9207 (https://doi.org/10.37807/GBMF9207) supported the research of S.C.-L. and F.R. The Margarita Salas Grant for the training of young doctors 2021URV-MS-20 supported the research of S.C.-L.

REFERENCES

Anthenelli, M., Jasien, E., Edwards, R., Bailey, B., Felts, B., Katira, P., Nulton, J., Salamon, P., Rohwer, F., Silveira, C. B., & Luque, A. (2020). Phage and bacteria diversification through a prophage acquisition ratchet. *bioRxiv*. https://doi.org/10.1101/2020.04.08.028340

Bashkirtseva, I., & Ryashko, L. (2018). Stochastic Sensitivity Analysis of Noise-Induced Extinction in the Ricker Model with Delay and Allee Effect. *Bull Math Biol*, *80*(6), 1596–1614. https://doi.org/10.1007/s11538-018-0422-6

Brum, J. R., Hurwitz, B. L., Schofield, O., Ducklow, H. W., & Sullivan, M. B. (2016). Seasonal time bombs: dominant temperate viruses affect Southern Ocean microbial dynamics. *The ISME Journal*, *10*(2), 437–449. https://doi.org/10.1038/ismej.2015.125

Bury, T. M., Sujith, R. I., Pavithran, I., Scheffer, M., Lenton, T. M., Anand, M., & Bauch, C. T. (2021). Deep learning for early warning signals of tipping points. *Proceedings of the National Academy of Sciences*, *118*(39), e2106140118. https://doi.org/doi:10.1073/pnas.2106140118

Cairns, B. J., Timms, A. R., Jansen, V. A. A., Connerton, I. F., & Payne, R. J. H. (2009). Quantitative Models of In Vitro Bacteriophage–Host Dynamics and Their Application to Phage Therapy. *PLOS Pathogens*, *5*(1), e1000253. https://doi.org/10.1371/journal.ppat.1000253

Cheng, H., Zhang, H., Spötl, C., Baker, J., Sinha, A., Li, H., Bartolomé, M., Moreno, A., Kathayat, G., Zhao, J., Dong, X., Li, Y., Ning, Y., Jia, X., Zong, B., Ait Brahim, Y., Pérez-Mejías, C., Cai, Y., Novello, V. F., … Edwards, R. L. (2020). Timing and structure of the Younger Dryas event and its underlying climate dynamics. *Proceedings of the National Academy of Sciences*, *117*(38), 23408–23417. https://doi.org/doi:10.1073/pnas.2007869117

Cheng, K., Zhao, Y., Du, X., Zhang, Y., Lan, S., & Zhengli, S. (2007). Solar radiation-driven decay of cyanophage infectivity, and photoreactivation of the cyanophage by host cyanobacteria. *Aquatic Microbial Ecology*, *48*, 13–18. https://doi.org/10.3354/ame048013

Cushing, J., Dennis, B., Desharnais, R., & Costantino, R. (1998). Moving toward an unstable equilibrium: saddle nodes in population systems. *Journal of Animal Ecology*, *67*(2), 298–306. https://doi.org/10.1046/j.1365-2656.1998.00194.x

De, K., MacLeod, M., Karambelkar, V., Jencson, J. E., Chakrabarty, D., Conroy, C., Dekany, R., Eilers, A.-C., Graham, M. J., Hillenbrand, L. A., Kara, E., Kasliwal, M. M., Kulkarni, S. R., Lau, R. M., Loeb, A., Masci, F., Medford, M. S., Meisner, A. M., Patel, N., … Vanderburg, A. (2023). An infrared transient from a star engulfing a planet. *Nature*, *617*(7959), 55–60. https://doi.org/10.1038/s41586-023-05842-x

De Paepe, M., & Taddei, F. (2006). Viruses' Life History: Towards a Mechanistic Basis of a Trade-Off between Survival and Reproduction among Phages. *PLoS Biology*, *4*(7), e193. https://doi.org/10.1371/journal.pbio.0040193

Ditlevsen, P., & Ditlevsen, S. (2023). Warning of a forthcoming collapse of the Atlantic meridional overturning circulation. *Nature Communications*, *14*(1), 4254. https://doi.org/10.1038/s41467-023-39810-w

Folke, C., Carpenter, S. R., Walker, B., Scheffer, M., Chapin, T., & Rockström, J. (2010). Resilience Thinking Integrating Resilience, Adaptability and Transformability. *Ecology and Society*, *15*(4). http://www.jstor.org/stable/26268226

Gutenkunst, R. N., Waterfall, J. J., Casey, F. P., Brown, K. S., Myers, C. R., & Sethna, J. P. (2007). Universally Sloppy Parameter Sensitivities in Systems Biology Models. *PLoS Computational Biology*, *3*(10), e189. https://doi.org/10.1371/journal.pcbi.0030189

Hastings, A., Abbott, K. C., Cuddington, K., Francis, T., Gellner, G., Lai, Y.-C., Morozov, A., Petrovskii, S., Scranton, K., & Zeeman, M. Lou. (2018). Transient phenomena in ecology. *Science*, *361*(6406), eaat6412. https://doi.org/doi:10.1126/science.aat6412

Hayes, W. B. (2007). Is the outer Solar System chaotic? *Nature Physics*, *3*(10), 689–691. https://doi.org/10.1038/nphys728

Hindmarsh, A. C. (1983). *ODEPACK, A Systematized Collection of ODE Solvers,* (R. S. Stepleman, M. Carver, R. Peskin, W. F. Ames, & R. Vichnevetsky, Eds.; Vol. 1, pp. 55–64). Scientific Computing.

Kannoly, S., Oken, G., Shadan, J., Musheyev, D., Singh, K., Singh, A., & Dennehy, J. J. (2023). Single-Cell Approach Reveals Intercellular Heterogeneity in Phage-Producing Capacities. *Microbiology Spectrum*, *11*(1). https://doi.org/10.1128/spectrum.02663-21

Kevorkian, J., & Cole, J. D. (1981). Limit Process Expansions Applied to Ordinary Differential Equations. In J. Kevorkian & J. D. Cole (Eds.), *Perturbation Methods in Applied Mathematics* (pp. 17–104). Springer New York. https://doi.org/10.1007/978-1-4757-4213-8_2

Laskar, J., & Gastineau, M. (2009). Existence of collisional trajectories of Mercury, Mars and Venus with the Earth. *Nature*, *459*(7248), 817–819. https://doi.org/10.1038/nature08096

Luque, A., & Silveira, C. B. (2020). Quantification of Lysogeny Caused by Phage Coinfections in Microbial Communities from Biophysical Principles. *MSystems*, *5*(5). https://doi.org/10.1128/mSystems.00353-20

Lyons, T. W., Reinhard, C. T., & Planavsky, N. J. (2014). The rise of oxygen in Earth's early ocean and atmosphere. *Nature*, *506*(7488), 307–315. https://doi.org/10.1038/nature13068

Margulis, L., & Sagan, D. (1997). *Microcosmos: Four Billion Years of Microbial Evolution*. University of California Press.

Oro, D., Alsedà, L., Hastings, A., Genovart, M., & Sardanyés, J. (2023). Social copying drives a tipping point for nonlinear population collapse. *Proceedings of the National Academy of Sciences*, *120*(11), e2214055120. https://doi.org/doi:10.1073/pnas.2214055120

Panahi, S., Do, Y., Hastings, A., & Lai, Y.-C. (2023). Rate-induced tipping in complex high-dimensional ecological networks. *Proceedings of the National Academy of Sciences*, *120*(51), e2308820120. https://doi.org/doi:10.1073/pnas.2308820120

Pedersen, E. J., Koen-Alonso, M., & Tunney, T. D. (2020). Detecting regime shifts in communities using estimated rates of change. *ICES Journal of Marine Science*, *77*(4), 1546–1555. https://doi.org/10.1093/icesjms/fsaa056

Petzold, L. (1983). Automatic Selection of Methods for Solving Stiff and Nonstiff Systems of Ordinary Differential Equations. *SIAM Journal on Scientific and Statistical Computing*, *4*. https://doi.org/10.1137/0904010

Rabinovich, M. I., Varona, P., Selverston, A. I., & Abarbanel, H. D. I. (2006). Dynamical principles in neuroscience. *Reviews of Modern Physics*, *78*(4), 1213–1265. https://doi.org/10.1103/RevModPhys.78.1213

Rinaldi, S., & Scheffer, M. (2000). Geometric Analysis of Ecological Models with Slow and Fast Processes. *Ecosystems*, *3*(6), 507–521. https://doi.org/10.1007/s100210000045

Roach, D. R., Leung, C. Y., Henry, M., Morello, E., Singh, D., Di Santo, J. P., Weitz, J. S., & Debarbieux, L. (2017). Synergy between the Host Immune System and Bacteriophage Is Essential for Successful Phage Therapy against an Acute Respiratory Pathogen. *Cell Host Microbe*, *22*(1), 38-47.e4. https://doi.org/10.1016/j.chom.2017.06.018

Rocha, J. C., Peterson, G., Bodin, Ö., & Levin, S. (2018). Cascading regime shifts within and across scales. *Science*, *362*(6421), 1379–1383. https://doi.org/doi:10.1126/science.aat7850

Scheffer, M. (2009). *Critical Transitions in Nature and Society*. Princeton University Press. https://doi.org/10.2307/j.ctv173f1g1

Scheffer, M., Bascompte, J., Brock, W. A., Brovkin, V., Carpenter, S. R., Dakos, V., Held, H., van Nes, E. H., Rietkerk, M., & Sugihara, G. (2009). Early-warning signals for critical transitions. *Nature*, *461*(7260), 53–59. https://doi.org/10.1038/nature08227

Seekell, D. (2016). Passing the point of no return. *Science*, *354*(6316), 1109. https://doi.org/doi:10.1126/science.aal2188

Seekell, D. A., Carpenter, S. R., Cline, T. J., & Pace, M. L. (2012). Conditional Heteroskedasticity Forecasts Regime Shift in a Whole-Ecosystem Experiment. *Ecosystems*, *15*(5), 741–747. http://www.jstor.org/stable/23253689

Seekell, D. A., Carpenter, S. R., & Pace, M. L. (2011). Conditional Heteroscedasticity as a Leading Indicator of Ecological Regime Shifts. *The American Naturalist*, *178*(4), 442–451. https://doi.org/10.1086/661898

Seekell, D. A., Cline, T. J., Carpenter, S. R., & Pace, M. L. (2013). Evidence of alternate attractors from a whole-ecosystem regime shift experiment. *Theoretical Ecology*, *6*(3), 385–394. https://doi.org/10.1007/s12080-013-0183-7

Silveira, C. B., Luque, A., & Rohwer, F. (2021). The landscape of lysogeny across microbial community density, diversity and energetics. *Environmental Microbiology*, *23*(8), 4098–4111. https://doi.org/10.1111/1462-2920.15640

Strogatz, S. H. (2015). *Nonlinear dynamics and chaos: with applications to physics, biology, chemistry, and engineering* (2nd ed.). Westview Press. https://search.library.wisc.edu/catalog/9910223127702121

Suttle, C. A., & Chen, F. (1992). Mechanisms and Rates of Decay of Marine Viruses in Seawater. *Applied and Environmental Microbiology*, *58*(11), 3721–3729. https://doi.org/10.1128/aem.58.11.3721-3729.1992

Virtanen, P., Gommers, R., Oliphant, T. E., Haberland, M., Reddy, T., Cournapeau, D., Burovski, E., Peterson, P., Weckesser, W., Bright, J., van der Walt, S. J., Brett, M., Wilson, J., Millman, K. J., Mayorov, N., Nelson, A. R. J., Jones, E., Kern, R., Larson, E., … SciPy, C. (2020). SciPy 1.0: fundamental algorithms for scientific computing in Python. *Nature Methods*, *17*(3), 261–272. https://doi.org/10.1038/s41592-019-0686-2

Weitz, J. S. (2016). *Quantitative viral ecology: Dynamics of viruses and their microbial hosts*. Princeton University Press.

TABLES

Table 1. Model parametrization. The columns provide the range and scenario values for the model parameters, agents' concentrations, and observational (obser.) times. (*) For the agents' concentrations, the scenarios correspond to the initial values; scenarios with two lines of initial values correspond to the transient dynamics case (tr.) and the quasi-equilibrium case (q.-eq.).

	Growth rate, r (h)	Infection rate, a (ml·h^{-1})	Burst size, c (phages)	Decay rate, m (h^{-1})	*Bacteria concentration, B (cells·ml^{-1})	*Phage concentration P (phages·ml^{-1})	Obser. time, τ (h)
Ranges	$3\cdot10^{-5}$–6	$7\cdot10^{-10}$–$1\cdot10^{-6}$	2–5,000	10^{-3}–0.8	$1\cdot10^{-4}$–$8\cdot10^{9}$	$1\cdot10^{-4}$–$2\cdot10^{10}$	0.8 – 16,800
Scenario1	Laboratory case of fast growing bacteria (*E. coli*-like) and lytic phage (T4-like)						
	0.9	$3\cdot10^{-8}$	50	$1.5\cdot10^{-3}$	10^{3}	10^{4}	14
Scenario 2	Environmental (marine-like) case of slow growing bacteria and fast decaying phage (UV exposure)						
	$3.2\cdot10^{-5}$	$1\cdot10^{-10}$	225	$1\cdot10^{-1}$	$6.7\cdot10^{7}$	$1\cdot10^{0}$	260
Scenario 3	Environmental (enriched coastal-like) case of relatively fast-growing bacteria and fast decaying phage						
	0.1	$3\cdot10^{-9}$	50	$1\cdot10^{-1}$	$2.65\cdot10^{3}$ (tr.) $6\cdot10^{5}$ (q-eq)	$4.93\cdot10^{4}$ (tr.) $6\cdot10^{6}$ (q-eq)	300
Scenario 4	Laboratory with deep ocean-like case of slow growing bacteria and slow decaying phage						
	$3.2\cdot10^{-5}$	$3\cdot10^{-8}$	50	$1.5\cdot10^{-3}$	$8.5\cdot10^{5}$ (tr.) $1\cdot10^{3}$ (q.-eq)	$3\cdot10^{3}$ (tr.) $1\cdot10^{4}$ (q.-eq)	13

FIGURES

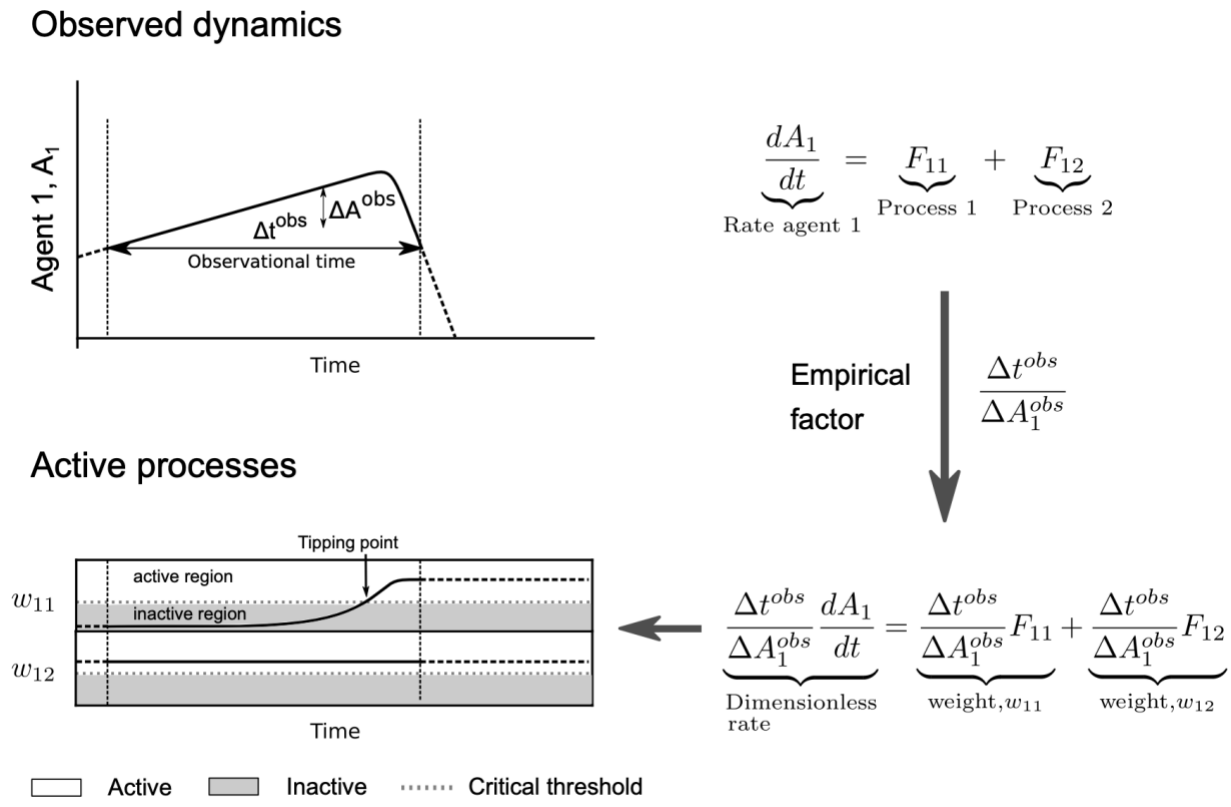

Figure 1: Observational principle and its mathematical application. (Top left panel) The observational principles is based on the fact that observations occur within a finite observational time, Δt^{obs}, and finite perceived observational relevant change, ΔA^{obs}. (Right panel) The observational principle leads to an observational rate (empirical factor) normalizing the processes (F_{ij}) involved in the dynamics of each agent, yielding to the observable weights, w_{ij}. (Bottom left panel) When a weights is above the threshold value (horizontal dotted line), the observer will perceive that the associated weight is relevant (white region). If it is below the threshold, the associate process is perceived as irrelevant (grey region).

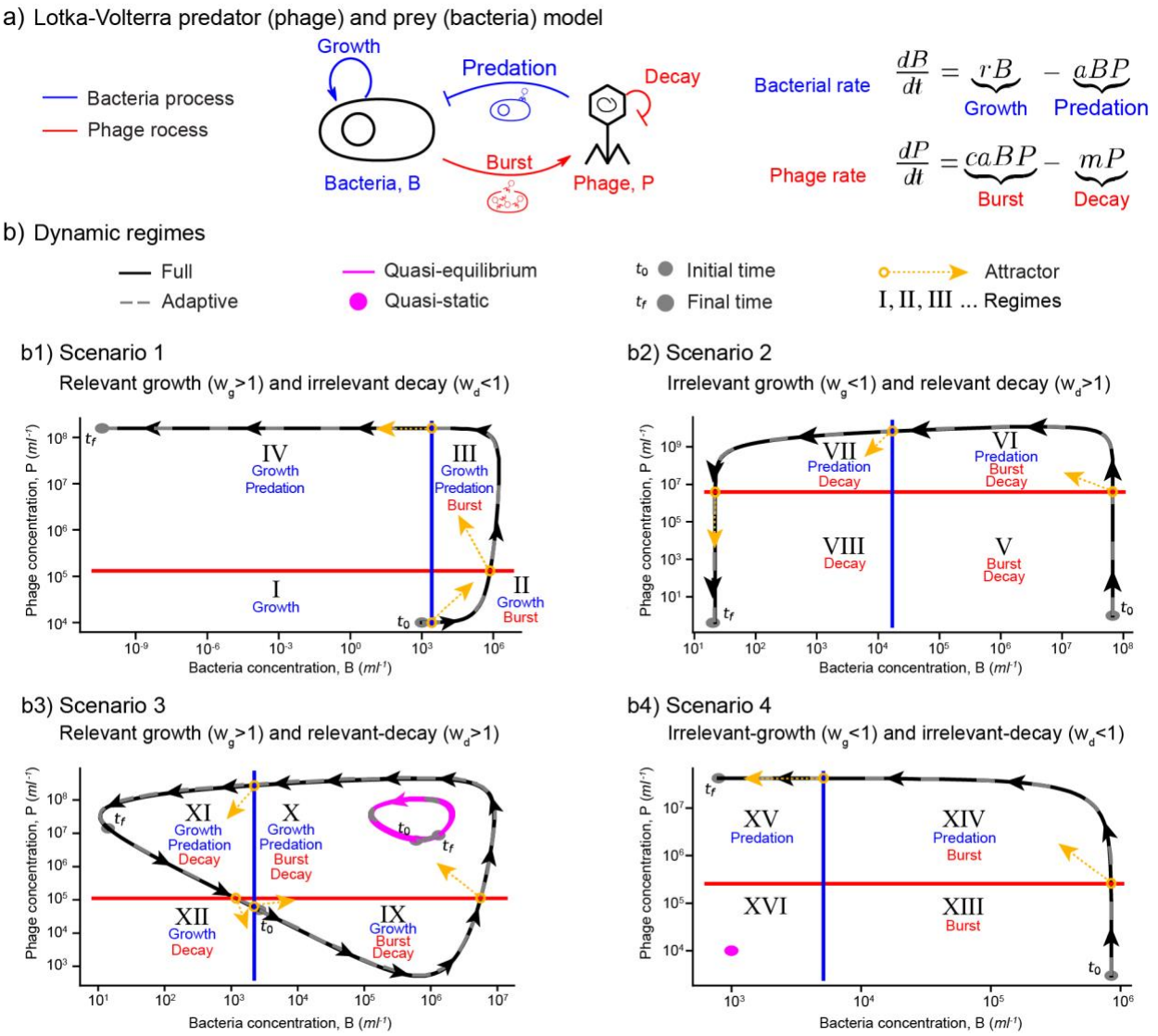

Figure 2. Phage-bacteria dynamic model and regimes. a) Diagram of the four processes involved in the phage-bacteria dynamics and the associated Lotka-Volterra model. The processes associated with the bacteria are displayed in blue and those with the phage are in red. b) Dynamic regimes for the phage-bacteria model for the four scenarios (b1 to b4) determined by the combination of growth and decay processes predicted to be relevant or irrelevant. Each plot displays the phage concentration versus the bacteria concentration. The black curves correspond to the trajectories of the full model with the black arrows indicating the time direction. The solid magenta curves display quasi-equilibrium and quasi-static trajectories. The grey dots are the

initial and end times. The vertical (blue) and horizontal (red) lines represent the bacteria (B_c) and phage (P_c) critical concentrations. Each regime (quadrant) is labeled with a Roman numeral and displays the associated relevant processes. The dashed grey curves display the trajectories from the adaptive Boolean model. The parameters for the trajectories are listed in Table 1.

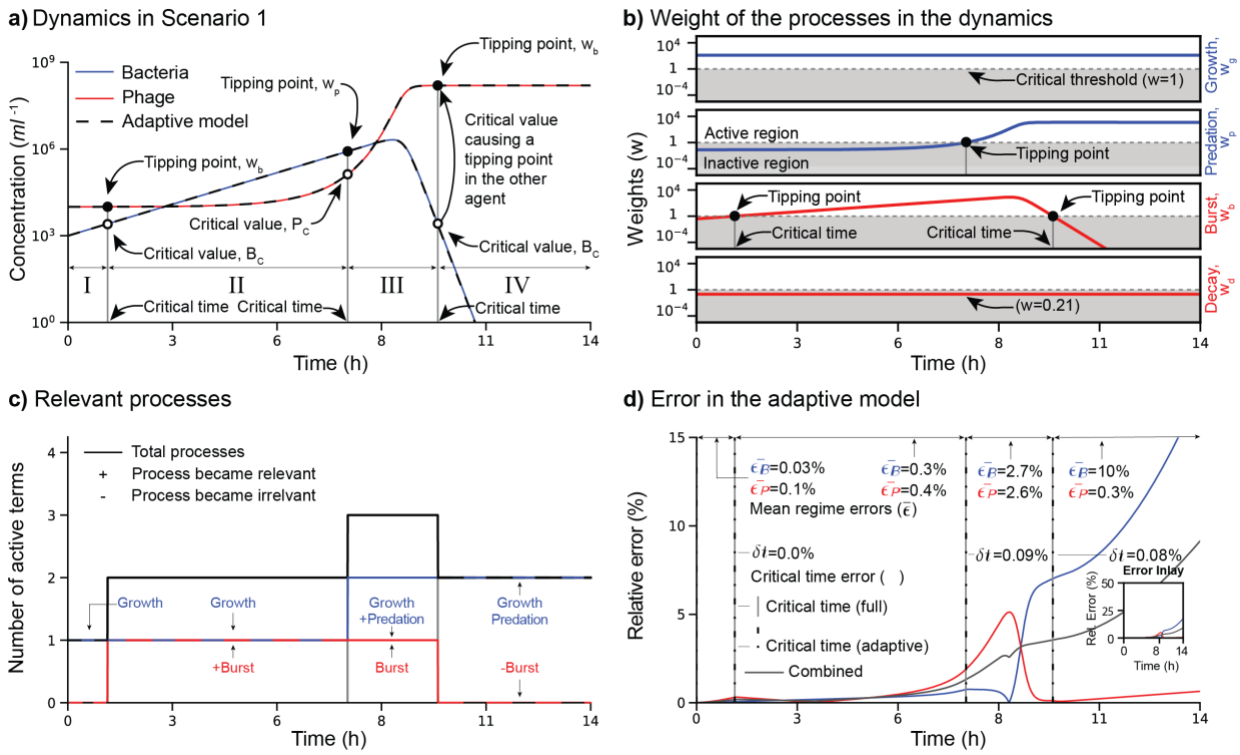

Figure 3. Transient dynamics for Scenario 1. a) Bacteria (blue) and phage (red) dynamics across the observational time. The vertical grey lines indicate the critical times when a critical value (open circle) is predicted to activate the tipping point (black circle), making a process relevant or irrelevant and changing the dynamic regime (Roman numerals, see Figure 2b1). The dashed line is the approximated dynamics obtained from the adaptive Boolean model (only relevant processes). b) Weight of each process throughout the dynamics. The horizontal dashed line is the critical threshold (w_{th}). The relevant region (above the threshold) is white and the irrelevant region (below the threshold) is grey. c) Relevant processes throughout the dynamics. The black line displays the total number of processes. The plus and minus symbols indicate, respectively, processes that became relevant and irrelevant when changing the dynamic regime. d) Relative error of the adaptive Boolean model when integrating only the relevant processes in comparison with the full model. The black line corresponds to the average error of the bacteria (blue) and phage (red). The mean errors for each regime are displayed for bacteria, $\bar{\epsilon}_B$, and

phage, $\bar{\epsilon}_P$. The critical time error (δt) indicates the discrepancy between the full (black vertical lines) and adaptive (dashed grey vertical lines) models for the time when a dynamic regime changes. The inset displays the relative error for a larger scale.

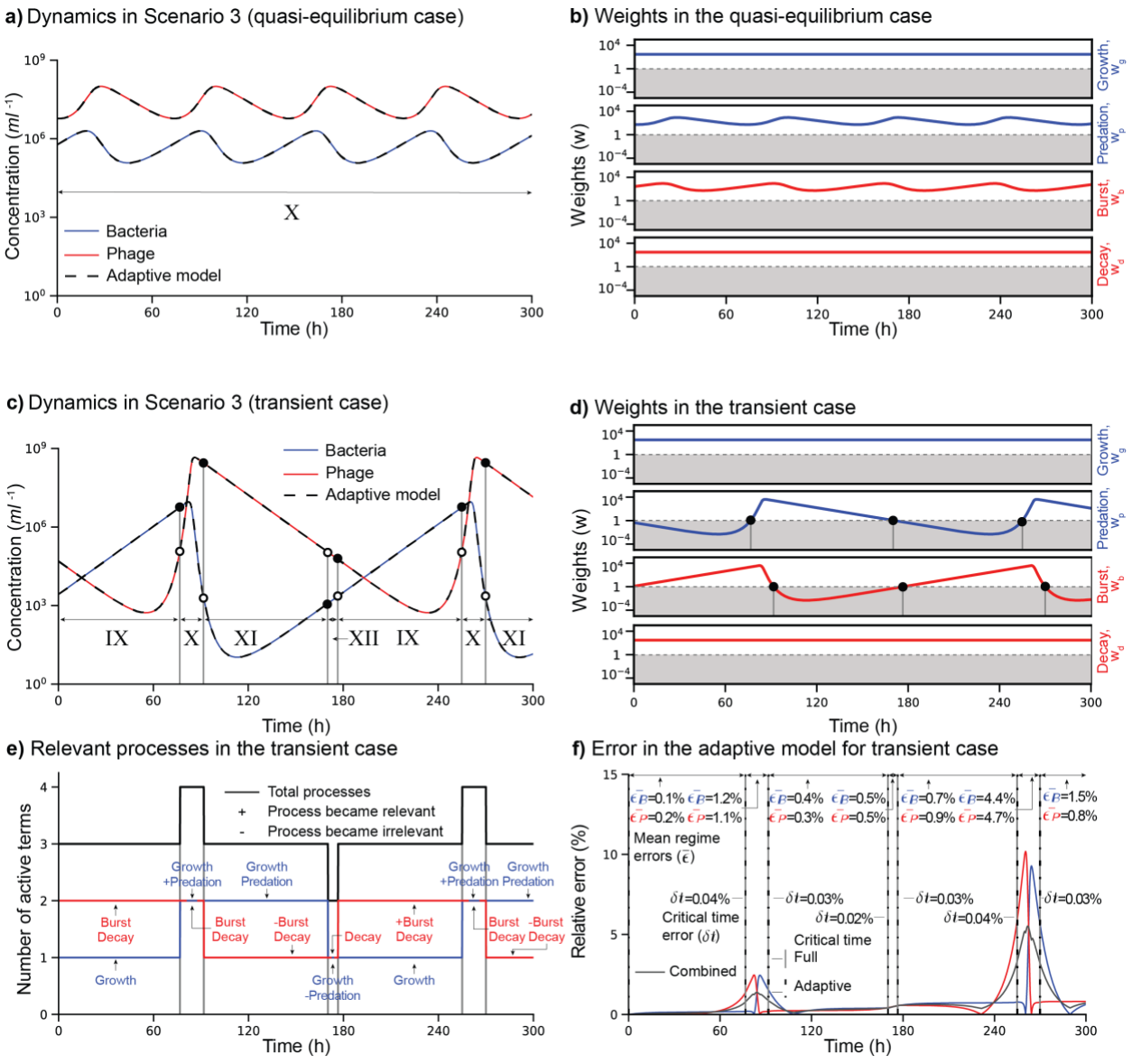

Figure 4. Quasi-equilibrium and transient dynamics for Scenario 3. a-b) Dynamics and weights for the quasi-equilibrium case. c-f) Dynamics, weights, relevant processes, and relative errors for the transient dynamic case. The symbols in each panel are analogous to those displayed and described in Figure 3. The parameters for this simulated scenario are in Table 1.

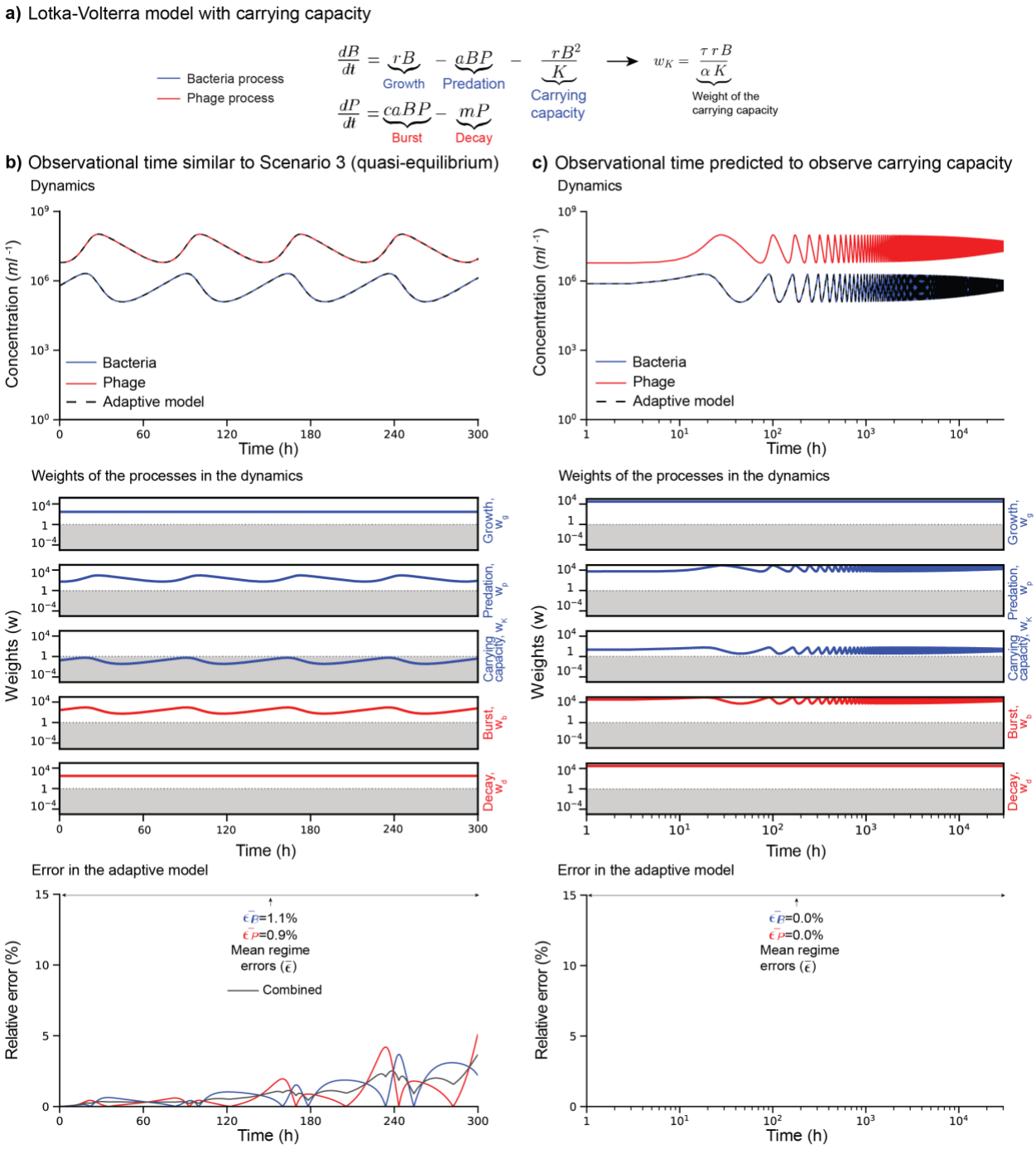

Figure 5. Phage-bacteria model with added carrying capacity process. a) Differential equation for the model indicating the bacteria processes in blue and the phage processes in red. The expression for w_K corresponds to the weight of the carrying capacity process. b) Dynamics (top), weights (middle), and relative error (bottom) when simulating the new model using the

parameters associated with the quasi-equilibrium case in Scenario 3 (Table 1 and Figures 4a-b). c) Analogous figures as in b) but using an observational time above the predicted critical observational time to observe the impact of the carrying capacity process in the dynamics.